Experimental study of compressive properties parallel to grain of glulam

Totsuka *et al. Journal of Wood Science* (2022) 68:33
https://doi.org/10.1186/s10086-022-02040-7

Journal of Wood Science

ORIGINAL ARTICLE Open Access

Experimental study of compressive properties parallel to grain of glulam

Marina Totsuka[1*], Robert Jockwer[2], Hiro Kawahara[3], Kenji Aoki[4] and Masahiro Inayama[4]

Abstract

This paper describes results and analysis of experiment of compression behavior parallel to grain of glulam (Norway Spruce, Japanese cedar, and Japanese cypress), especially in damage zones near loading plates and joints. To investigate the influence factors of physical properties and the mechanism of the damage zone near the loading plates or the joints, compression tests on 90 specimens and surface-measurement tests on 48 specimens were performed. As a result, it was observed that damage zones existed near the loading plates and the joints. The lengths of the damage zone of wood–wood joints are larger than that of wood–steel joints. The length of the damage zone was independent of the load and the height of the specimens. However, the length of the damage zone and its scatter increase as the width of the cross-section increases, as does the roughness on the contact surface. It was considered that the cause of the damage zone is the roughness on the contact surface and the length of the damage zone depends on the roughness on the contact surface. Therefore, the length of the damage zone depends on the processing accuracy on the contact surface and has an increasing trend as the contact-surface area increases. There was the size effect of the height of the specimens on the compressive strength because of knots.

Keywords: Glulam, Damage zone, Compression parallel to grain, Joints, Connections, Surface roughness, Timber

Introduction

In recent years, high-rise timber buildings have been built in the world. In timber buildings, the deformations concentrate on the connections and the deformations of the connections were complex [1]. In connections, since the deformations under compression perpendicular to the grain are bigger than the deformations under compression parallel to the grain by anisotropy of wood, the deformations under compression parallel to the grain are often ignored. However, in high-rise timber buildings, we need to consider the deformation under compression parallel to the grain as well.

The heterogeneity of the strains in members loaded in compression parallel to the grain of clear specimens was reported in papers [2, 3] (Choi et al. and Dahl and Malo). It is observed that the largest strains are allocated near the loading plates [4] (Zink et al.), which create a zone often called the "damage zone" as shown in Fig. 1. The zone between these damage zones is referred to as the "middle zone". Xavier et al. [5] and Brabec et al. [6] investigated the behavior of the damage zones, e.g., the length and the modulus of elasticity, in small clear specimens. They defined the damage zone as a zone with a high variation strain (0.2–1.7%) at 50% of a maximum strength. In addition, Totsuka et al. [7] reported the heterogeneity of the strains of large-sawn-timbers specimens and showed the possibility that the increasing length of damage zone with the increase of the widths of the loaded area and the length of the damage zone does not change when the full height of the specimens increases. The compression strength parallel to the grain of large-scale specimens of glulam is presented by Fryer et al. [8] and Flaig et al. [9]. The report by Fryer et al. [8] presented the presence of a size effect of the glulam specimens. The report by Flaig et al. [9] presented the results of the experimental test

*Correspondence: mtotsuka@chiba-u.jp

[1] Department of Architecture, Graduate School of Engineering, Chiba University, 1-33 Yayoi-cho, Inage-ku, Chiba-shi, Chiba, Japan
Full list of author information is available at the end of the article

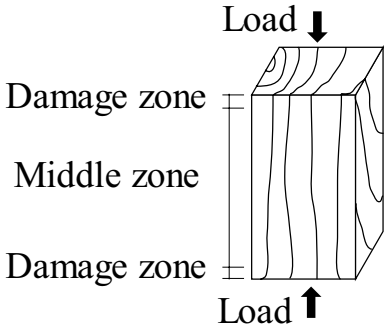

Fig. 1 Explanation of damage zone and middle zone

with end-grain contact joints in glulam and indicated that damage zone occurred around the end-grain contact joints. However, there is no evaluation method of damage zone and the behavior of the damage zones in glulam specimens remains unsolved so far.

In this present work, the compressive property parallel to the grain of glulam was investigated. The aims of this work are as follows:

(1) To clarify the relationship between physical properties in the damage zone and the roughness of contact surfaces and the influence factors of physical properties in the damage zone.

(2) To study the mechanism of the damage zone in various types of end-grain contact joints.

Materials and methods

Specimens

Table 1 shows an overview of the test series of glulam specimens. The specimens were made from glulam of Norway spruce (*Picea abies*) of quality GL30h according to SS-EN 14080:2013 [10], and Japanese cedar (*Cryptomeria japonica*) of quality E65-F255 and Japanese cypress (*Chamaecyparis obtusa*) of quality E95-F315 according to JAS (Japanese Agricultural Standards) [11]. The thickness of the glulam laminae was 42 mm for Norway spruce and 30 mm for Japanese cedar and Japanese cypress. The width of the glulam laminae was the same as the specimen width.

A total of 90 specimens were prepared by manufacturing 6 or 4 specimens per series; see Table 1. The test parameters are the size of the specimens and the type of joints, shown in Fig. 2. The specimens of series 20-3sSp had a 9-mm steel plate. The actual dimensions and weight of each specimen were measured before testing. The moisture content of specimens after testing was measured by a dual-function moisture meter. The density of specimens was measured immediately before the testing. The specimens had typical wood characteristics, adhesive layers, and finger joints, however, the

Table 1 Overview of test series

Series	Species	#	Specimen size [mm]		Joint type	Moisture content [%]
			Cross section	Height		
2.5-1Sp	Norway spruce	6	25 × 25	100	–	7.5–10.6
10-1Sp			100 × 100	100	–	
20-1Sp			200 × 200	100	–	
20-05Sp			200 × 200	50	–	
20-3Sp			200 × 200	300	–	
20-3bSp		4	200 × 200	300	Butt (parallel)	
20-3bxSp			200 × 200	300	Butt (cross)	
20-3sSp			200 × 200	300	Steel plate	
2.5-1Ce	Japanese cedar	6	25 × 25	100	–	10.9–11.3
10-1Ce			100 × 100	100	–	
20-1Ce			200 × 200	100	–	
20-2Ce			200 × 200	200	–	
2.5-1Cy	Japanese cypress	6	25 × 25	100	–	8.2–11.3
10-1Cy			100 × 100	100	–	
20-1Cy			200 × 200	100	–	
20-2Cy			200 × 200	200	–	

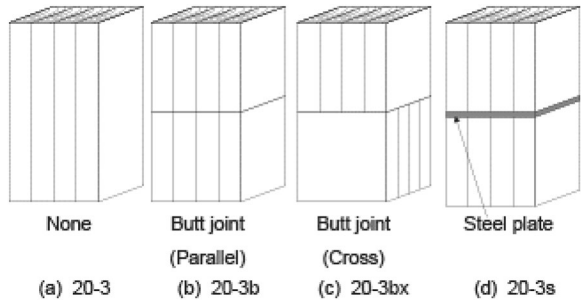

Fig. 2 Test parameters of joint types

specimens of series 2.5-1Sp, 2.5-1Ce, and 2.5-1Cy did not exhibit visual defects (knots and cracks) and did not have adhesive layers and finger joints.

Test methods

For the spruce specimens, the compression tests of the specimens were carried out on a load frame for compressive strength tests with an in-line 3000 kN load cell and a spherically seated loading-head, an in-line displacement transducer under displacement control at a rate of 1 mm/min. The 3D deformations and local strains in two adjacent surfaces were determined by the digital image correlation (DIC) system ARAMIS (ARAMIS, GOM, Braunschweig, Germany) [12], equipped with dual digital cameras. ARAMIS captured images at a frequency of 1 Hz during the test.

For the cedar and cypress specimens, the compression tests were carried out on a load frame for compressive strength tests with an in-line 3000 kN load cell, a spherically seated loading-head, and four displacement

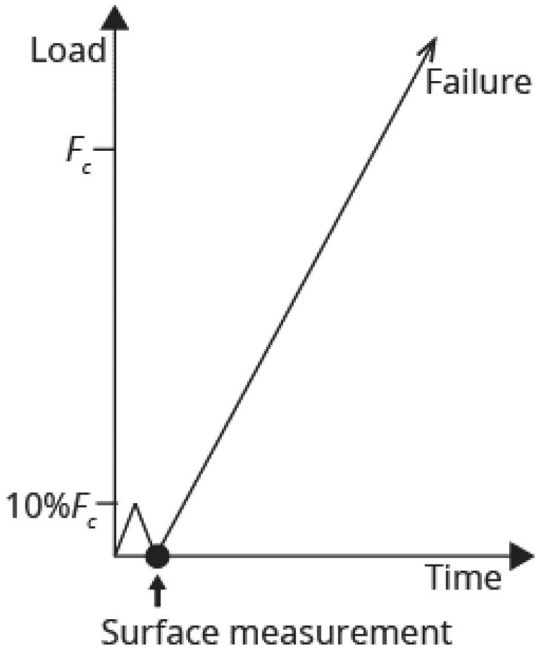

Fig. 3 Loading and surface measurement cycle of cedar and cypress specimens

transducers to measure the displacement of the total height of the specimens under displacement control at a rate of 1 mm/min. The loading and surface measurement cycle is shown in Fig. 3. The roughness on the contact surfaces was measured at 10% of the previously published strength F_c (F_c is 35 N/mm^2 for cedar and 40 N/mm^2 for cypress) [13], by a hybrid measuring instrument for surface roughness and contour measurement (SV-C4100H8, Mitutoyo, Kanagawa, Japan)

Fig. 4 Surface measurement of cedar and cypress specimens

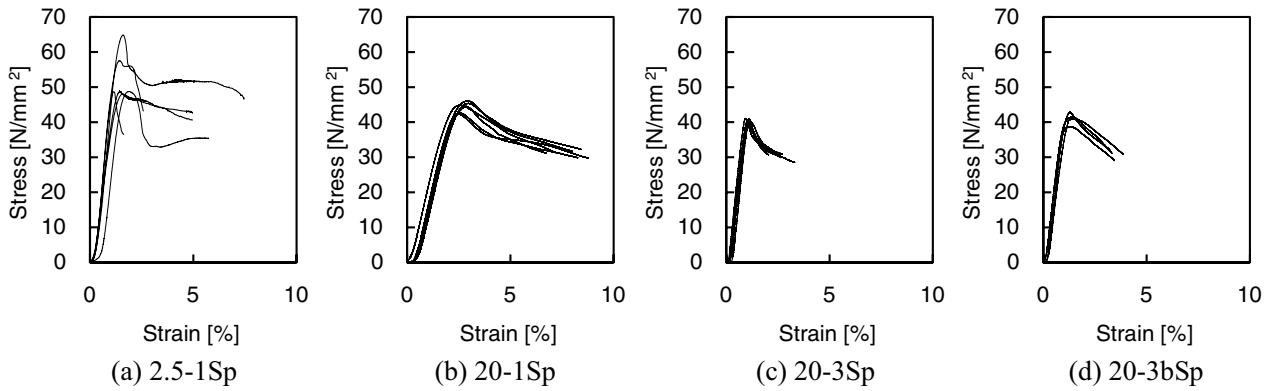

Fig. 5 Typical stress–strain curves of the specimens

as shown in Fig. 4. It is the device to measure surface roughness by tracing the surface with a stylus. The 2D deformations and local strains in a surface were determined by the DIC system by a digital camera. A 2D optical system captured images at a frequency of 0.2 Hz during the test. The images were processed with the DIC software (GOM correlate, GOM, Braunschweig, Germany) [9]. This software uses an automated computer algorithm to determine local displacements and strains according to deformation images. For all specimens, a speckle pattern, which consisted of black dots on a white surface, was painted on the face of these specimens face.

Test results and discussion

Experimental results

The stress (σ_c) and strain (ε) were calculated from Eqs. 1 and 2:

$$\sigma_c = \frac{P}{A}, \tag{1}$$

$$\varepsilon = \frac{\Delta l}{H}, \tag{2}$$

where P is the applied compression load measured by the load cell, A is the cross-sectional area of the specimens, Δl is the average of the deformation in the full height of the specimens measured by the in-line displacement transducer and H is the initial height of the specimens.

Figure 5 shows the typical stress–strain curves of the specimens. The stress–strain curves except for series 2.5-1Sp, 2.5-1Ce, and 2.5-1Cy were homogeneous. It was considered that these specimens consist of the multiple laminations. Series 2.5-1Sp, 2.5-1Ce, and 2.5-1Cy consisted of single laminae and these results were more inconsistent than that of the other specimens.

Figure 6 shows the typical failure mechanisms. For all specimens, compressive failure was kink band failure [14]. Kink band and large deformation were observed near the loading plates and the butt joints or in the middle zone. In particular, in the specimens having relatively large knots, kink bands occurred across the knots; see Fig. 6. The adhesive layers and finger joints are not the origin of the failure.

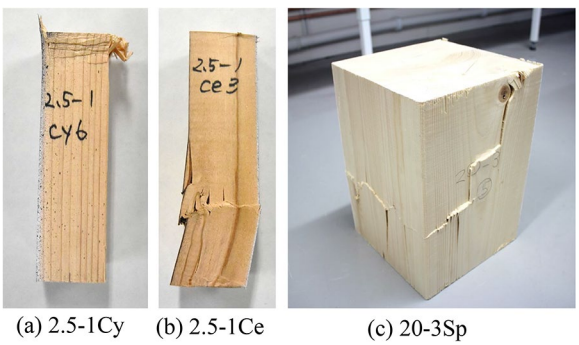

Fig. 6 Typical failure mechanisms: **a** kink band failure on damage zone, **b** kink band failure on damage zone and middle zone, **c** kink band failure on middle zone caused by knots

Size effects of compression strength and moduli

The strength (maximum stress) was calculated as the ratio between the maximum load (P_{max}) and the loaded area of the specimen (A):

$$f_{c,0} = \frac{P_{max}}{A}. \tag{3}$$

According to the equilibrium and linear elastic constitutive equations, the following closed-form solution can be obtained for the identification of the longitudinal modulus of elasticity:

Table 2 Mean statistics of specimens

Sample statistics	Maximum stress $f_{c,0}$ [N/mm^2]							
	2.5-1Ce	**10-1Ce**	**20-1Ce**	**20-2Ce**	**2.5-1Cy**	**10-1Cy**	**20-1Cy**	**20-2Cy**
Quantity	6	6	6	6	6	6	6	6
Mean	31	33	34	33	47	44	45	44
CV [%]	6	5	2	3	5	3	2	5
	Longitudinal modulus of elasticity in full height $E_{L,f}$ [N/mm^2]							
Mean	4383	4432	5349	6649	6823	6284	8242	10,091
CV [%]	19	5	4	1	20	6	5	4
	Longitudinal modulus of elasticity in middle zone $E_{L,m}$ [N/mm^2]							
Mean	7549	8807	14,318	9722	14,966	15,247	22,575	14,847
CV [%]	12	14	34	8	11	15	18	8
Sample statistics	**Maximum stress $f_{c,0}$ [N/mm^2]**							
	2.5-1Sp	**10-1Sp**	**20-1Sp**	**20-05Sp**	**20-3Sp**	**20-3bSp**	**20-3bxSp**	**20-3sSp**
Quantity	6	6	6	6	6	4	4	4
Mean	53	44	44	47	41	41	41	42
CV [%]	12	6	3	1	1	4	2	4
	Longitudinal modulus of elasticity in full height $E_{L,f}$ [N/mm^2]							
Mean	5327	4920	2507	1601	5510	2558	2381	2670
CV [%]	9	11	3	7	4	3	6	2
	Longitudinal modulus of elasticity in middle zone $E_{L,m}$ [N/mm^2]							
Mean	13,155	12,440	13,950	13,414	11,865	13,240	12,500	14,064
CV [%]	13	9	16	18	5	9	10	11

CV coefficient of variation

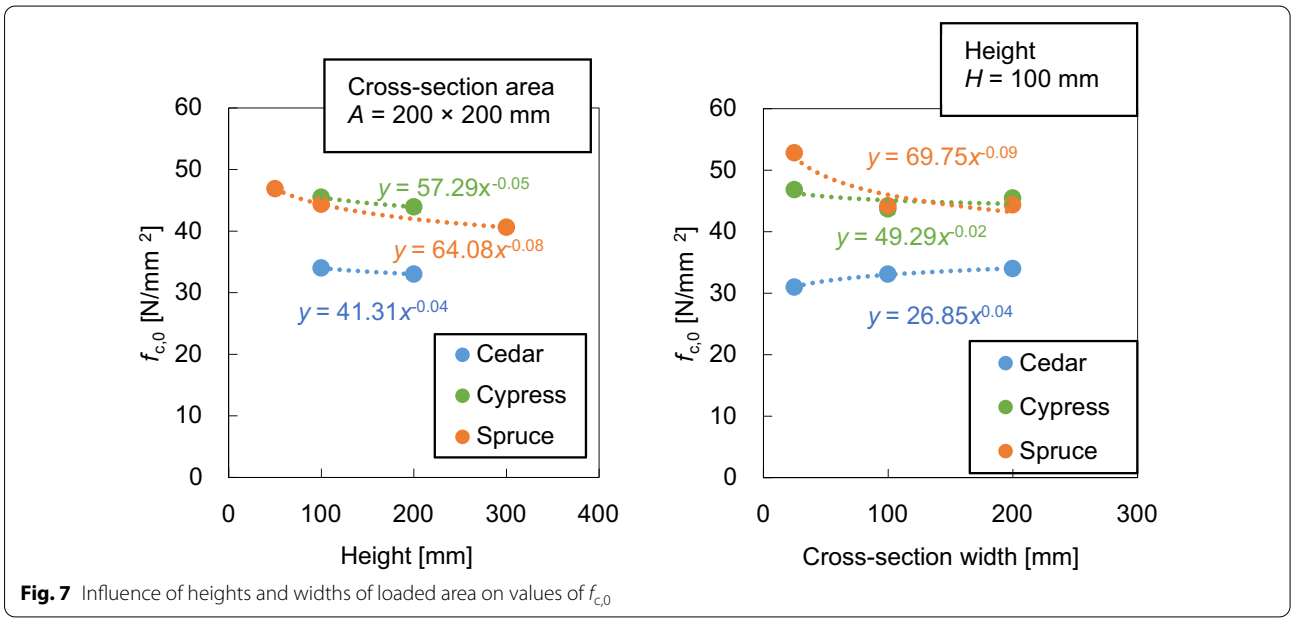

Fig. 7 Influence of heights and widths of loaded area on values of $f_{c,0}$

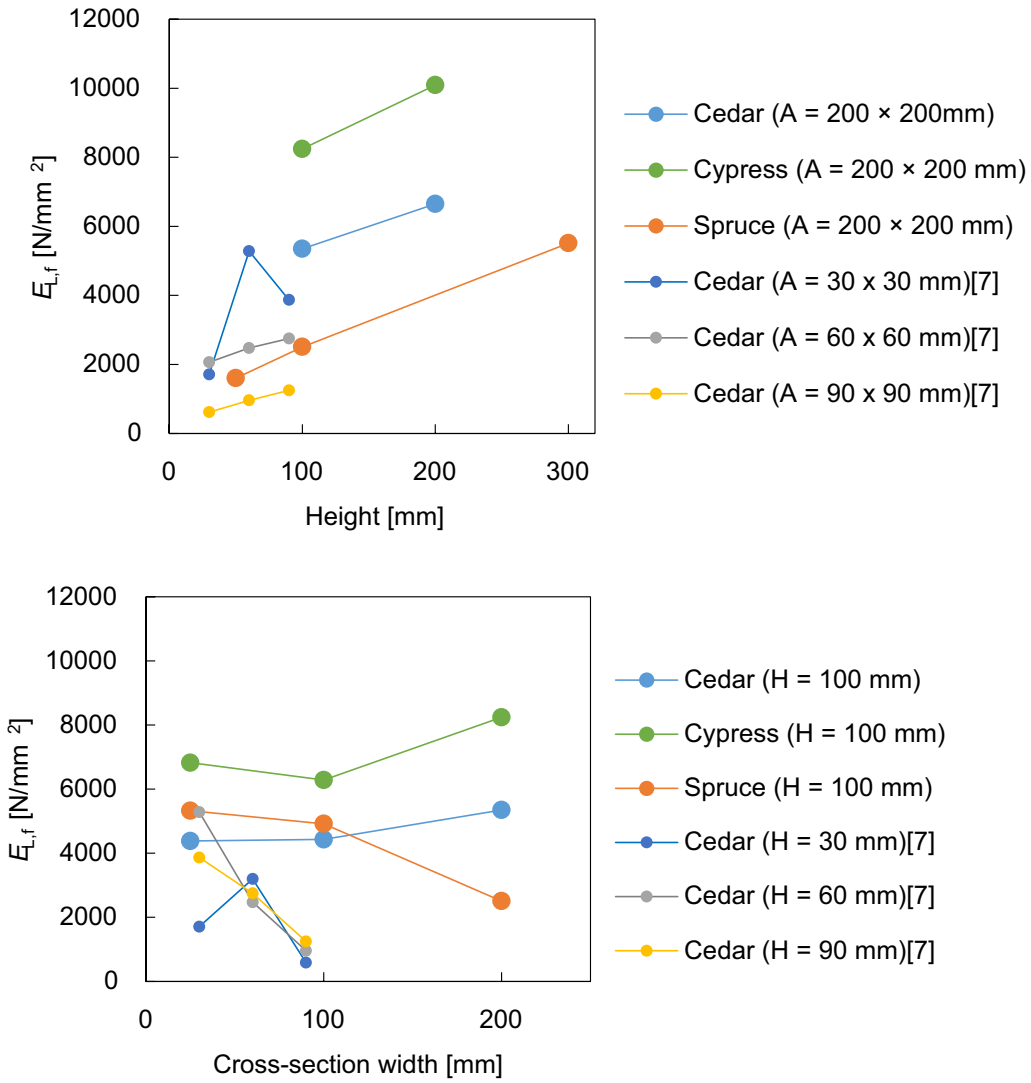

Fig. 8 Influence of heights and widths of cross-sectional area on values of $E_{L,f}$

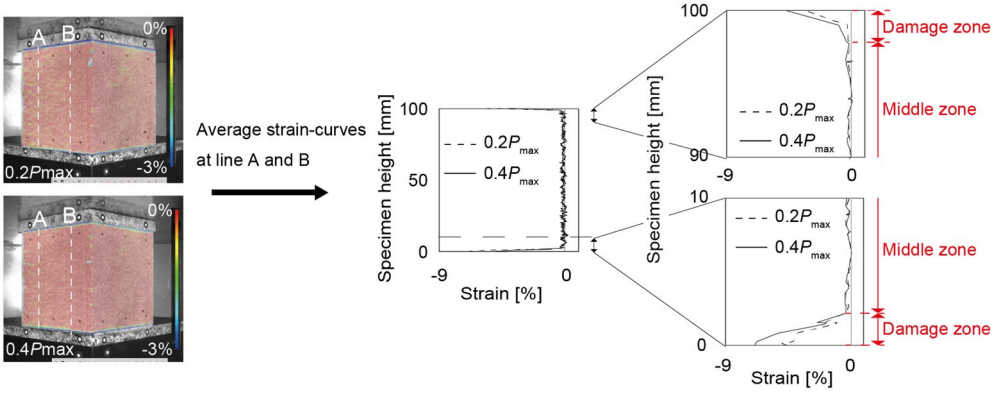

(a) Deformation fields of longitudinal strain (b) Average of the line A and B of 0.2 and 0.4 P_{max}

Fig. 9 Longitudinal strains of specimen 10-1Ce at 0.2 and 0.4 P_{max} by DIC

$$E_L = \frac{P}{A\varepsilon_1}, \tag{4}$$

where P is the applied compression load and ε_1 is the linear strain, from $0.2P_{\max}$ to $0.4\ P_{\max}$, along the longitudinal direction. In this study, two types of the E_L were calculated: (1) the longitudinal modulus of elasticity in full height ($E_{\mathrm{L,f}}$) using the ε_1 in the full information of the specimens measured by the displacement transducers; (2) the longitudinal modulus of elasticity in the middle zone ($E_{\mathrm{L,m}}$) using the ε_1 in the middle zone measured by the DIC.

Table 2 shows the statistics of the specimens. The values of $E_{\mathrm{L,m}}$ were independent of the dimensions (height and width) of the specimens and the joint types. The mean values of $E_{\mathrm{L,m}}$ were close to the literature values (7350 N/mm^2 for cedar and 11,700 N/mm^2 for spruce[13], but no literature value for cypress) and considered to be equivalent to Young's modulus measured with a strain gauge or displacement meter attached to the middle of the test specimen. The mean values of $E_{\mathrm{L,m}}$ of series 20-1Ce and 20-1Cy were bigger than that of the other series. The reason for this is unknown and further consideration will be needed to yield any findings about it.

Figure 7 presents the influence of the heights and the widths of the loaded area on the values of $f_{\mathrm{c,0}}$. These values indicate mean values of the specimens with a cross-sectional area of 200 × 200 mm for the influence of the heights and with a height of 100 mm for the influence of the widths of the loaded area. With a method of least squares fitting, it was found that the strength $f_{\mathrm{c,0}}$ is proportional to the height of the specimen raised to the power of − 0.05 (the spruce specimens), − 0.04 (the cedar specimens), and − 0.08 (the cypress specimens); see Fig. 7. Studies by Fryer et al. [8] also found a reduction in compressive strength of glulam, parallel to the grain, with increased member size. The size effect of the cross-sectional area on the compressive strength $f_{\mathrm{c,0}}$ was very small. We have reported that there is no size effect in the $f_{\mathrm{c,0}}$ of the solid timber specimens [7]. The main reason of the strength reduction may be related to knots because the solid timber specimens did not have knots, whereas all the glulam specimens excluding the 2.5-1 specimens had knots.

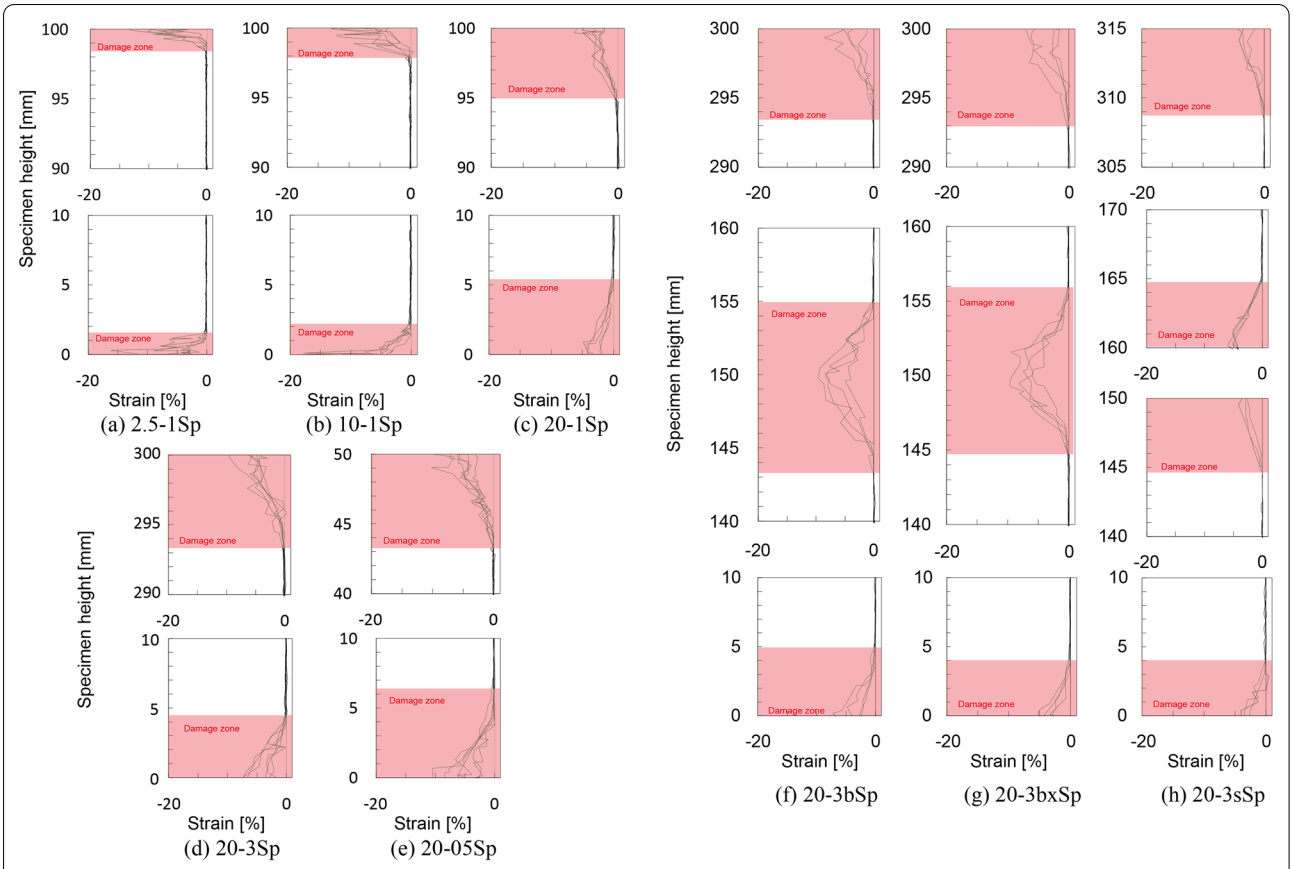

Fig. 10 Longitudinal strains distribution of specimens near loading plates in 0.2 $P_{\max}$

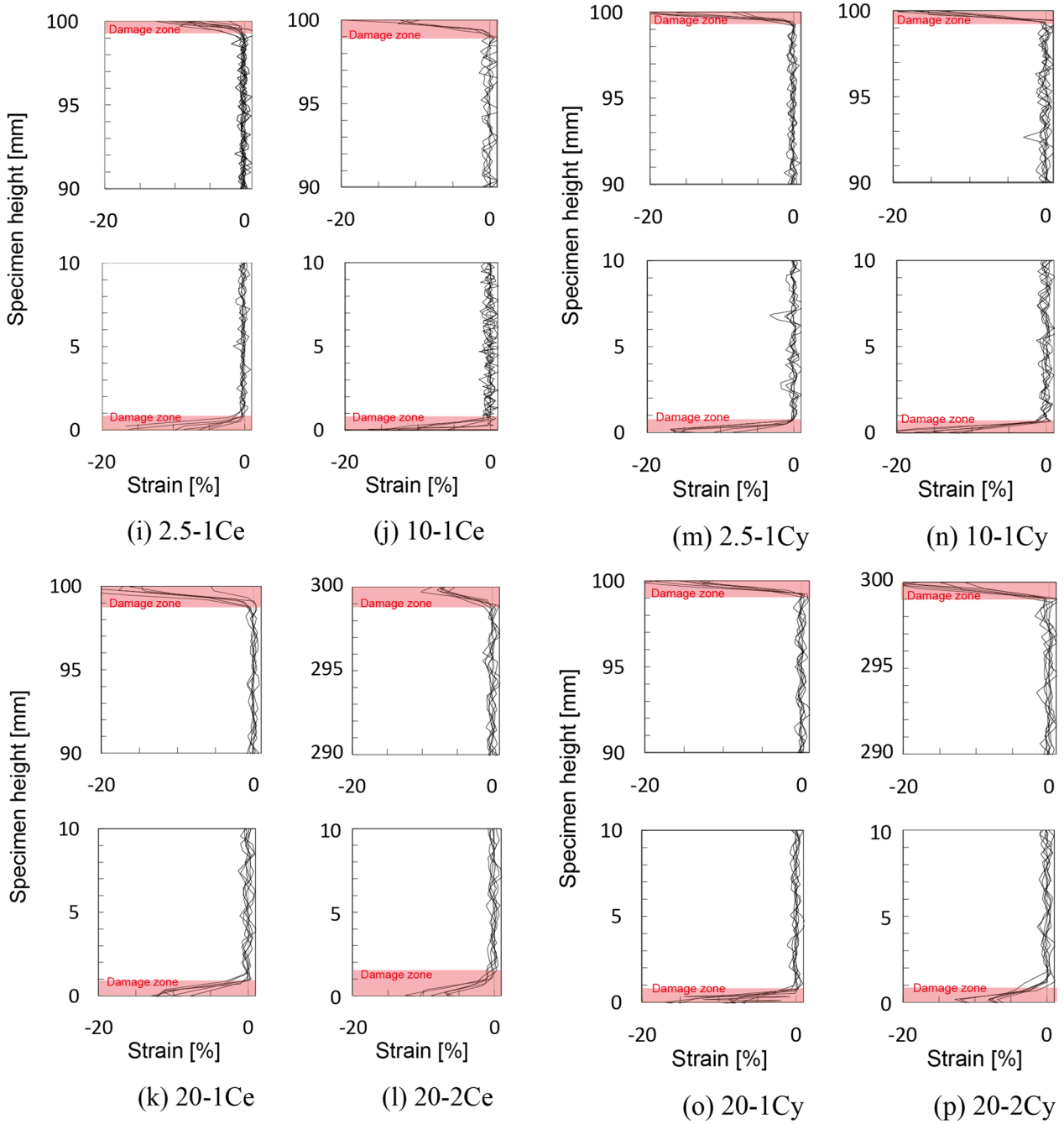

Fig. 10 continued

Figure 8 presents the influence of the heights and the widths of the loaded area on the values of $E_{L,f}$. The test results of solid timber of cedar [7] are also shown in Fig. 8. These values indicate mean values of the specimens with a cross-sectional area of 200×200 mm and 30×30–90×90 mm [7] for the influence of the heights and with a height of 100 mm and 30–90 mm [7] for the influence of the widths of the loaded area. The E

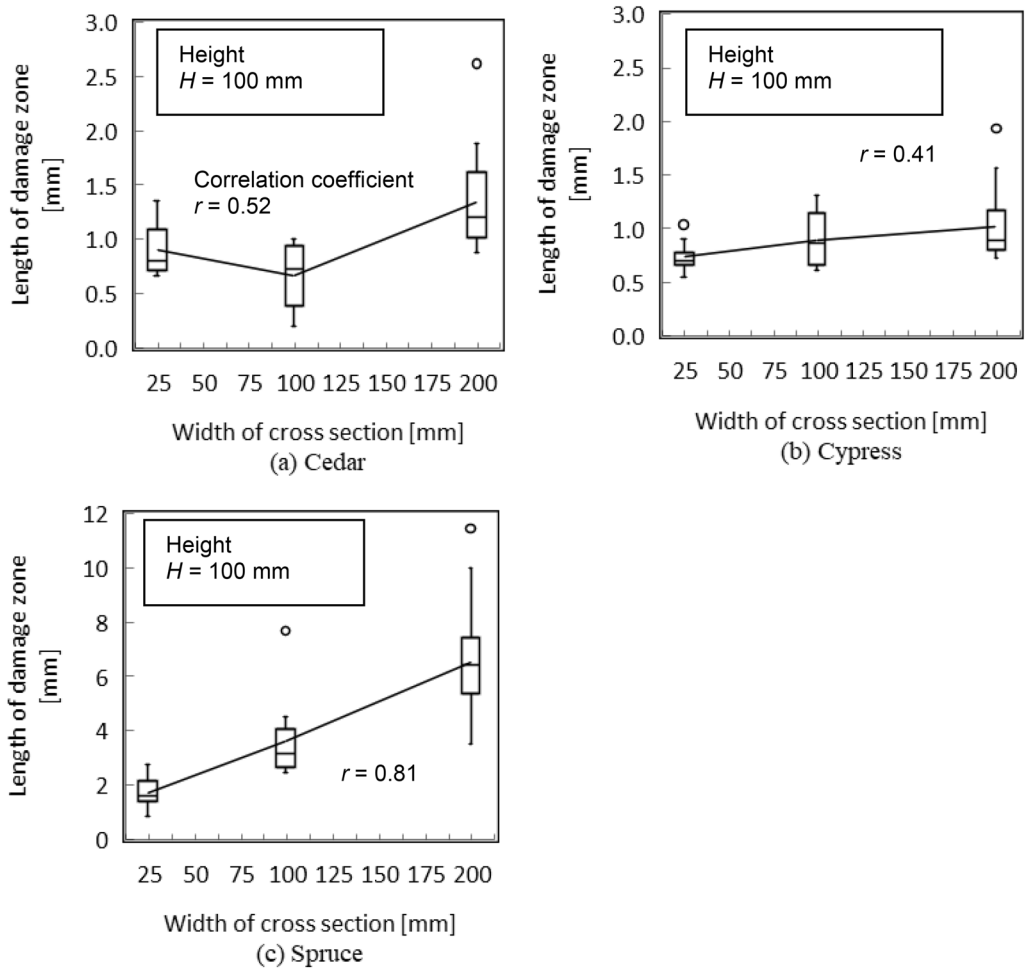

Fig. 11 Length of damage zone of specimens of varying widths of cross-section

$_{L,f}$ had an increasing trend as the height increased. This can be explained by that the lengths of the damage zone do not change when the full height of the specimens increases. The $E_{L,f}$ had an increasing trend as the width of the loaded area decreased in the spruce specimens and solid timber. This can be explained by the increasing lengths of the damage zone with the increase of the widths of the loaded area. However, the $E_{L,f}$ did not have an increasing trend in the cedar and cypress specimens. To clarify the mechanism of the damage zone, the damage zones were analyzed in the following.

Strain field characterization and length of the damage zone

Figure 9 shows an example of the deformation field of the longitudinal strain and the average of the longitudinal strain curves at lines A and B at 20% and 40% of the maximum load (P_{max}) of the series 10-1Sp by DIC. A damage zone near the loading plates or the joints and the middle zone can be recognized. The strain in the damage zone had a gradual distribution along with the height and exponentially increases as the distance from the loading plate or the joint decreased. The phenomenon of the damage zone near the loading plates is in agreement with the observations made by Martin [6]. The maximum strain is dependent on the load, but the length of the damage zone at 20% of the P_{max} was almost the same as that at 40% of the P_{max}.

Figure 10 shows the longitudinal strain curves at 20% of the P_{max} of the specimens by DIC. The length of the damage zone seemed to be independent of the height, but the length increases as the loaded area increases. A

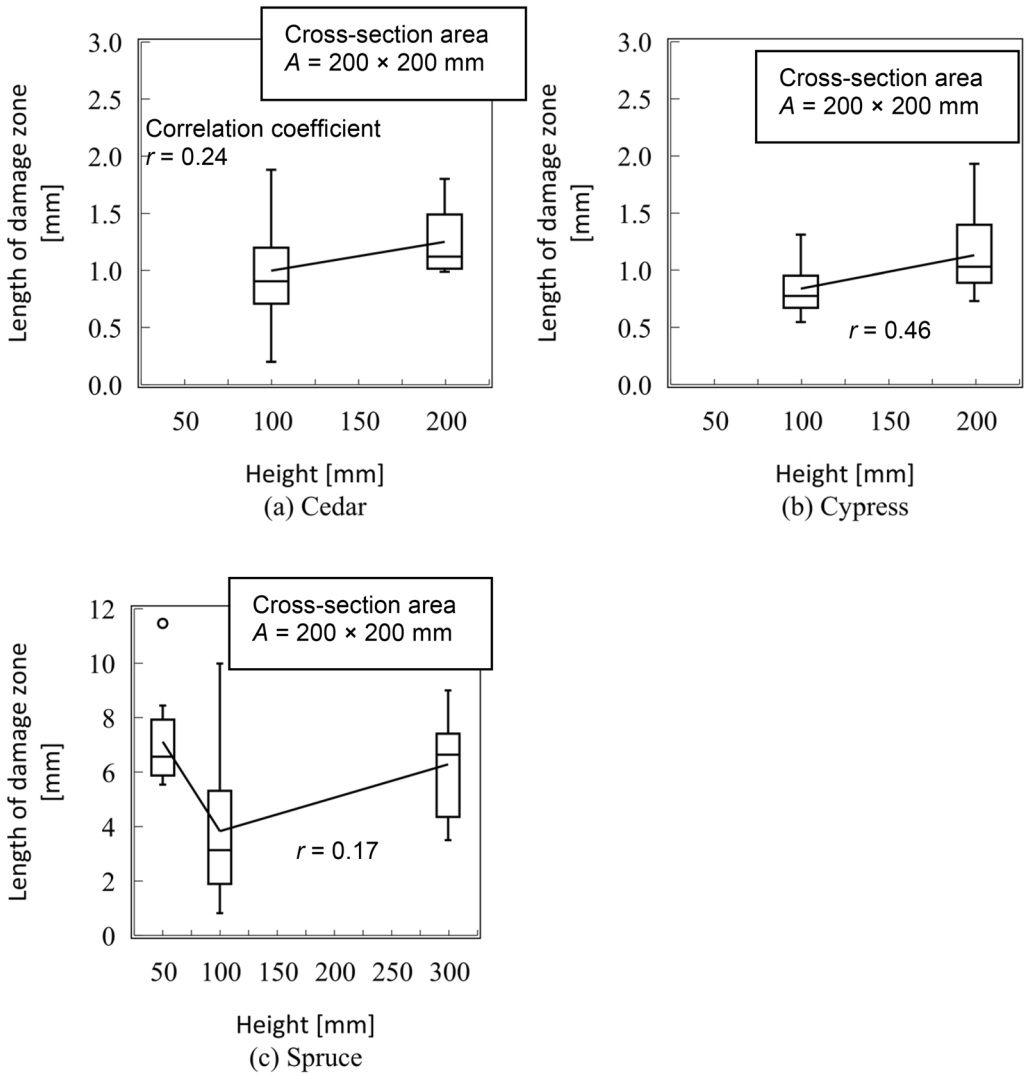

Fig. 12 Length of damage zone of specimens of varying heights

detailed discussion of the length of the damage zone is provided in Figs. 11, 12, 13. Figure 10f–h shows the longitudinal strain curves of wood–wood joints and wood–steel joints. Damage zones were also observed near the wood–wood joints and wood–steel joints, as well as near the loading plates.

Where the damage zone was defined at a strain ε_1 of −0.2% and less at 20% of P_{max}, the average lengths of the damage zone were 0.9 mm in 2.5-1Ce, 0.7 mm in 2.5-1Cy, 1.1 mm in 2.5-1Sp, 0.7 mm in 10-1Ce, 0.9 mm in 10-1Cy, 2.3 mm in 10-1Sp, 1.3 mm of the cedar specimens with 200 mm, 1.0 mm of the cypress specimens with 200 mm, and 4.7 mm of the spruce specimens with 200 mm width; see Fig. 11. Positive correlations were suggested between the length of damage zone and the width of the cross-section with correlation coefficients of +0.52 for the cedar specimens, +0.41 for the cypress specimens and +0.81 for the spruce specimens. The length of the damage zone and its scatter increase as the width of the cross-section increases. This trend was especially remarkable in the spruce specimens. It was probably because the spruce specimens were processed on a different machine and

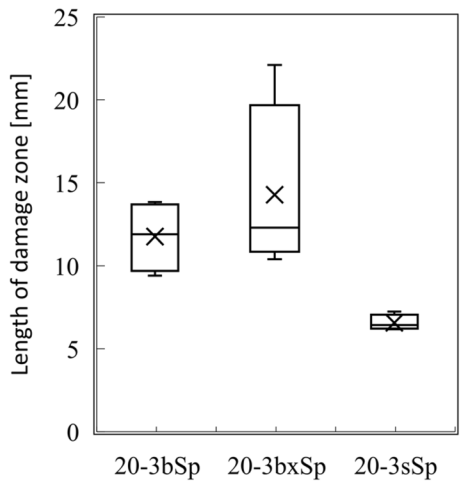

Fig. 13 Length of damage zone of specimens with wood–wood joints and wood–steel joints

the processing of the spruce specimens was rougher than that of the cedar and cypress specimens. The cedar and cypress specimens were processed on the same machine. The surface roughness of the contacted area is likely to increase as the cross-sectional area of the specimens increases. In other words, the length of the damage zone may depend on the accuracy of the processing machine. The details of the surface roughness on the contact surface were investigated in the following. On the other hand, lower or negligible correlations between the length of the damage zone and the height of the specimen were indicated with correlation coefficients of + 0.24 for the cedar specimens, + 0.46 for the cypress specimens and + 0.17 for the spruce specimens in Fig. 12. The length of the damage zone did not change when the height of the specimen changed.

Figure 13 shows the length of the damage zone near wood–wood joints and wood–steel joints. It was considered that the lengths of the damage zone of wood–wood joints are larger than that of wood–steel joints.

Surface roughness parameters

Regarding the cedar and cypress specimens, the profile curves on the contact surface were measured at 10% of design strength F_c as shown in Fig. 14. To discuss the surface roughness, profile parameters, P_a (Arithmetical mean height) and P_z (Maximum height of profile), were used according to ISO 4287 [15].

Figure 15 shows a relationship between the profile parameters and the cross-sectional area of the specimens. Positive correlations were suggested between the P_a and P_z and the width of the cross-section with correlation coefficients of + 0.77 (P_a) and + 0.60 (P_z) for the cedar specimens and + 0.78 (P_a) and + 0.81 (P_z) for the cypress specimens. The values of the P_a and P_z and its scatter increase as the width of the cross-section increases, as does the length of the damage zone. The mean values of the P_a in Fig. 15 especially similar to the length of the damage zone in Fig. 11.

Figure 16 shows a relationship between the profile parameters and the height of the specimens. Lower correlations between the P_a and P_z and the height of the specimen were indicated with correlation coefficients of + 0.58 (P_a) and + 0.54 (P_z) for the cedar specimens, + 0.47 (P_a and P_z) for the cypress specimens. Because it is probable that the length of the damage zone did not depend on the height but the cross-sectional area of the specimens as well as the P_a and P_z, it was considered that the cause of the damage zone is the roughness on the contact surface and the length of the damage zone depends on the roughness on the contact surface.

Conclusion

An experimental study on the compression behavior parallel to the grain in glulam specimens has been conducted to clarify the size effect of the compression strength, Young's modulus, and the behavior of the damage zone. There was the size effect of the height of the specimens on the compressive strength $f_{c,0}$ of glulam specimens. The size effect of the cross-sectional area on the compressive strength $f_{c,0}$

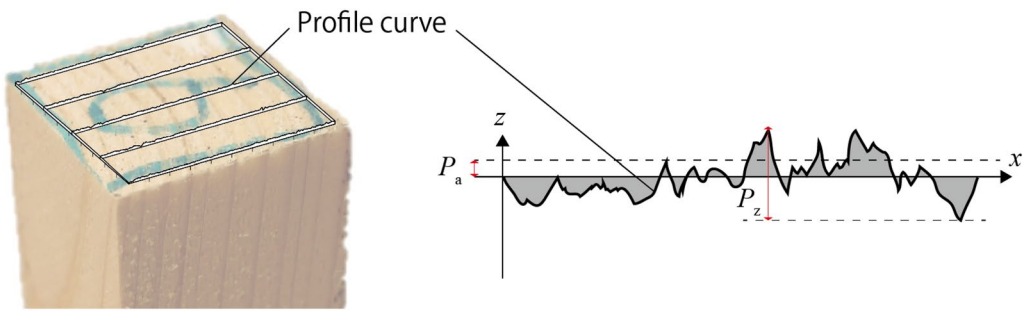

Fig. 14 Typical surface profile and profile parameters

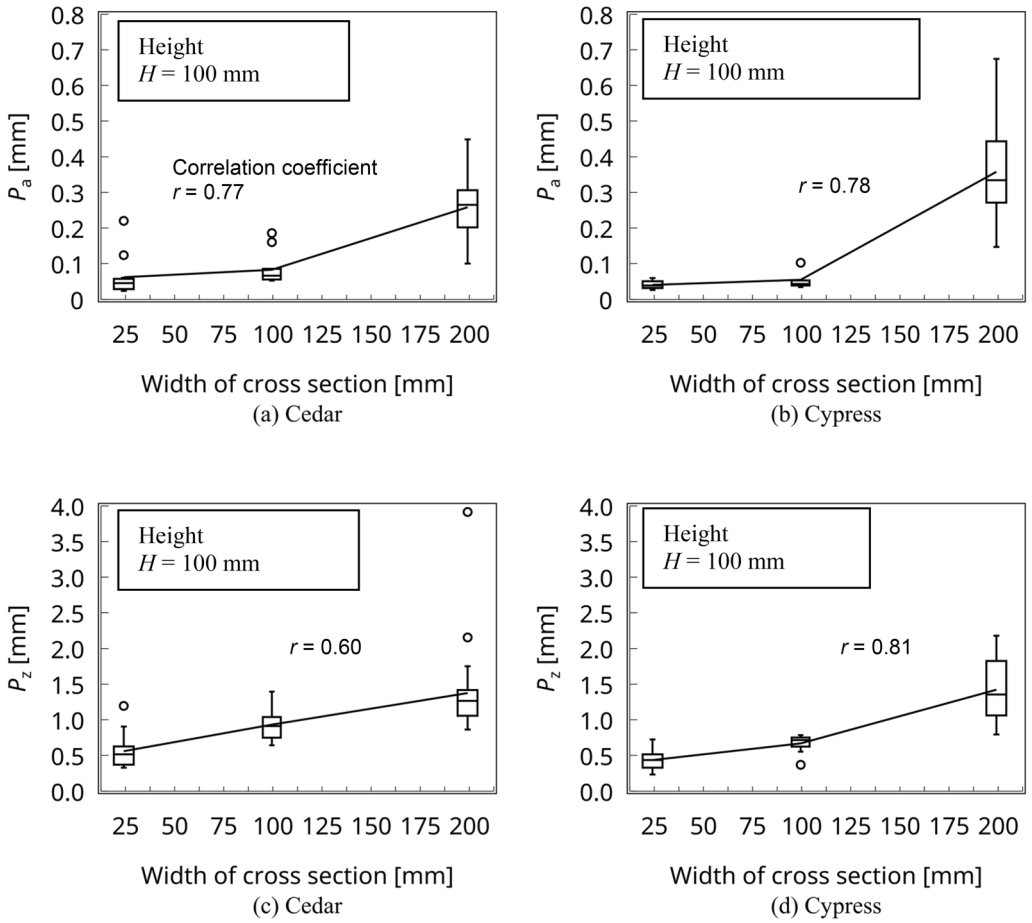

Fig. 15 Relationship between the profile parameters and the cross-sectional area of the specimens

was very small. The main cause of the strength reduction by the size effect of the height may be related to knots.

Damage zones existed near the loading plates and the joints. The length of the damage zone was independent of the load and the height, but the length increases as the loaded area increases. The lengths of the damage zone of wood–wood joints are larger than that of wood–steel joints. The length of the damage zone and its scatter increase as the width of the cross-section increases, as does the roughness on the contact surface. It was considered that the cause of the damage zone is the roughness on the contact surface and the length of the damage zone depends on the roughness on the contact surface. Therefore, the length of the damage zone depends on the processing accuracy on the contact surface and has an increasing trend as the contact-surface area increases. When we consider deformations of connections, we should consider the effect of the damage zone.

The values of moduli, $E_{\mathrm{L,m}}$, were independent of the dimensions (height and width) of the specimens and the joint types. The modulus $E_{\mathrm{L,f}}$ had an increasing trend as the height increased because the lengths of the damage zone did not change when the full height of the specimens increased. The $E_{\mathrm{L,f}}$ had an increasing trend as the width of the loaded area decreased because the length of the damage zone increased as the cross-sectional area increased.

It is a question of future study to make an evaluation method of the damage zone. In addition, future studies could fruitfully explore this issue further by applying this study to connections.

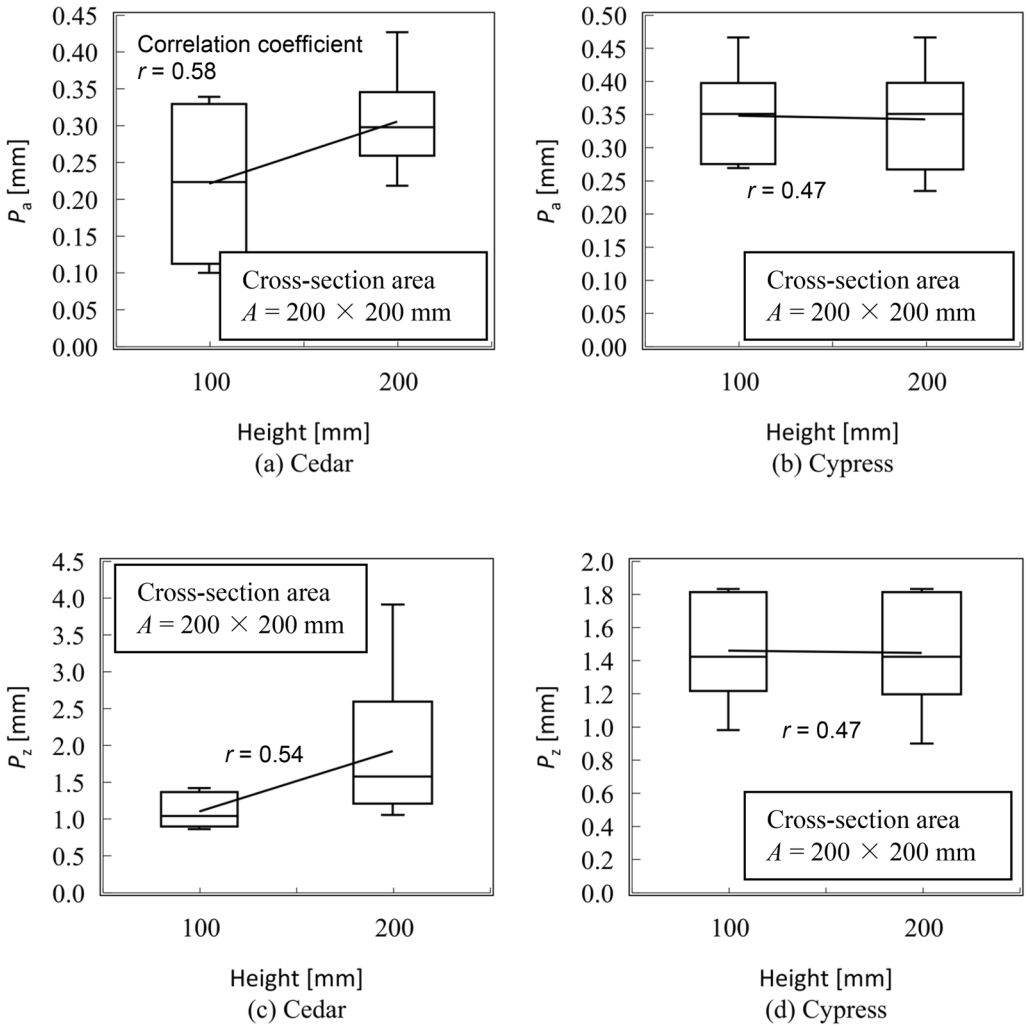

Fig. 16 Relationship between the profile parameters and the height of the specimens

Abbreviations
Glulam: Glued laminated timber; DIC: Digital image correlation; JAS: Japanese Agricultural Standards; CV: Coefficient of variation.

Acknowledgements
Some specimens of the experiments were prepared by Meiken Lamwood Corp. We are deeply grateful to Meiken Lamwood Corp.

Author contributions
MT, RJ, KA, and MI designed the experiments. MT, RJ and HK performed the experiments. MT and RJ analyzed the data. MT was a major contributor in writing the manuscript. All authors contributed to interpretation and discussed results. All authors read and approved the final manuscript.

Funding
This work was supported by Grant-in-Aid for JSPS Research Fellow Number JP19J13253.

Availability of data and materials
The datasets used and analyzed in the current study are available from the corresponding author on reasonable request.

Declarations

Competing interests
The authors declare that they have no competing interests.

Author details
[1]Department of Architecture, Graduate School of Engineering, Chiba University, 1-33 Yayoi-cho, Inage-ku, Chiba-shi, Chiba, Japan. [2]Division of Structural Engineering, Department of Architecture and Civil Engineering (ACE), Chalmers University of Technology, Sven Hultins Gata 6, 412 96 Gothenburg, Sweden. [3]Department of Architecture, School of Science and Technology for Future Life, Tokyo Denki University, 5 Senjuasahichou, Adachi-ku, Tokyo, Japan. [4]Department of Biomaterials Sciences, Graduate School of Agricultural and Life Sciences, The University of Tokyo, 1-1-1 Yayoi, Bunkyo-ku, Tokyo, Japan.

Received: 16 December 2021 Accepted: 30 May 2022
Published online: 11 June 2022

References

1. Jockwer R, Grönquist P, Frangi A (2021) Long-term deformation behaviour of timber columns: monitoring of a tall timber building in Switzerland. Eng Struct 234:111855. https://doi.org/10.1016/j.engstruct.2021.111855
2. Choi D, Thorpe JL, Hanna RB (1991) Image analysis to measure strain in wood and paper. Wood Sci Technol 25:251–262. https://doi.org/10.1007/BF00225465
3. Dahl KB, Malo KA (2009) Planar strain measurements on wood specimens. Exp Mech 49:575–586. https://doi.org/10.1007/s11340-008-9162-0
4. Zink AG, Davidson RW, Hanna RB (1995) Strain measurement in wood using a digital image correlation technique. Wood Fiber Sci 27(4):346–359
5. Xavier J, de Jesus AMP, Morais JJL, Pinto JMT (2011) Stereovision measurements on evaluating the modulus of elasticity of wood by compression tests parallel to the grain. Constr Build Mater 26(1):207–215. https://doi.org/10.1016/j.conbuildmat.2011.06.012
6. Brabec M, Tippner J, Sebera V, Milch J, Rademacher P (2015) Standard and non-standard deformation behavior of European beech and Norway spruce during compression. Holzforschung 69(9):1107–1116. https://doi.org/10.1515/hf-2014-0231
7. Totsuka M, Jockwer R, Aoki K, Inayama M (2021) Experimental study on partial compression parallel to grain of solid timber. J Wood Sci. https://doi.org/10.1186/s10086-021-01972-w
8. Fryer BK, Foster RM, Ramage MH (2018) Size effect of large scale timber columns. In: Proceedings of the 12th WCTE, Seoul, Korea, Republic of Korea, 20–23 August 2018.
9. Flaig M, Schmidt T, Blass HJ (2019) Compressive strength and stiffness of end grain contact joints in glulam and CLT. In: Proceedings of INTER 2019—Meeting 52, Tacoma, WA, 26–29 August 2019.
10. SS-EN 14080 (2013) Timber structures—Glued laminated timber and glued solid timber—requirements. Swedish Institute for Standards. Stockholm.
11. Japanese agricultural standards notice no. 1587 (2012) Glulam. Ministry of Agriculture. Forestry and Fisheries. Tokyo **(In Japanese)**
12. GOM Correlate (GOM GmbH, Germany). https://www.gom.com/en/products/gom-suite/gom-correlate-pro. Accessed 3 Mar 2022.
13. Ringyo-shikenjo, (ed) (1958) Mokuzai kogyo handbook. Maruzen, Tokyo
14. Benabou L (2010) Predictions of compressive strength and kink band orientation for wood species. Mech Mater 42(3):335–343. https://doi.org/10.1016/j.mechmat.2009.11.015
15. ISO 4287 (1998) Geometrical product specifications (GPS)—Surface texture: profile method—Terms, definitions and surface texture parameters. British Standards Institute, London

Publisher's Note